

Supporting information

1 Experimental section

1.1 Materials

High purity Sn (filamentous, 99.99%) was purchased from Zhongluo New Material Technology Co. Ltd. MWCNTs was obtained from Zhongke Times Nano. KNO_3 (solid) was derived from Guangdong Guanghua Sci-Tech Co. Ltd. and accurately configured into 2 mol/L KNO_3 solution. The Li^+ electrolyte was provided by Shanghai Songjing New Energy. 1 mol/L LiPF_6 was dissolved in ethylene carbonate/diethyl carbonate, containing 5 wt% fluoroethylene carbonate (EC/DEC (1:1 V:V)+5% FEC). All of the above samples can be used directly.

1.2 Characterizations

The crystalline structures of the prepared samples were characterized by X-ray diffraction (Germany-Bruck-D8 Advanced, scan rate of $10^\circ/\text{min}$). Raman spectroscopy (Microscopic laser Raman, in Via) and Fourier infrared spectroscopy (FT-IR, Nicolet 6700) confirmed the functional group structure. The specific surface area of composite materials was measured by Brunner-Emmet-Teller (BET) method (Tri-star II 3020, Micromeritics). The porosity features were analyzed by Barrette Joynere Halenda (BJH) way. The percentage of SnO_2 content was determined by thermogravimetric analysis (Germany-Nexi-TG 209F3) under air atmosphere from room temperature to 800°C . The morphologies and microstructure of materials were observed using SEM (Zeiss sigma300 + Oxford spectrum) and TEM (JEM-2100). The composition, and valence states of surficial elements were tested by X-ray photoelectron spectroscopy (XPS, America-ThermoFisher Nexsa).

1.3 Electrochemical measurements

The electrochemical properties of composite materials were tested through CHI 660e electrochemical workstation. The galvanostatic charge-discharge (GCD) measurements (range of 0.01–3.0 V), electrochemical impedance spectroscopy (EIS) (range of 0.01–100 kHz), cyclic voltammetry (CV) curves (range of 0.01–3.0 V) were put into effect. The active substance, acetylene black and carboxymethyl cellulose sodium (CMC) were mixed according to the mass ratio of 7:1.5:1.5, and milled to form a uniformly slurry with pure water as solvent to prepare the working electrode, then dried them in a vacuum oven at 80°C for 10 h. To prepare a specific cell, Li metal was the counter electrode, and 1 mol/L LiPF_6 (dissolved in EC/DEC (1:1 V:V)+5% FEC) was the electrolyte.

2 Material characterizations

2.1 FT-IR spectroscopy and SEM characterizations

The infrared spectrogram had obvious special peaks of Sn—O bond at low wave number, due to the formation of SnO_2 [S1]. The peaks of the remaining two high wave number segments were attributed to the formation of C—O and C=O (Figure S1(a)). Sn/ SnO_2 particles ranged in size between 15 and 30 nm (Figure S1(b)), which slightly larger than the particle size of SnO_2 @CNTs (Figure S1(c)). The particles were always stacked together, and the size was uniform.

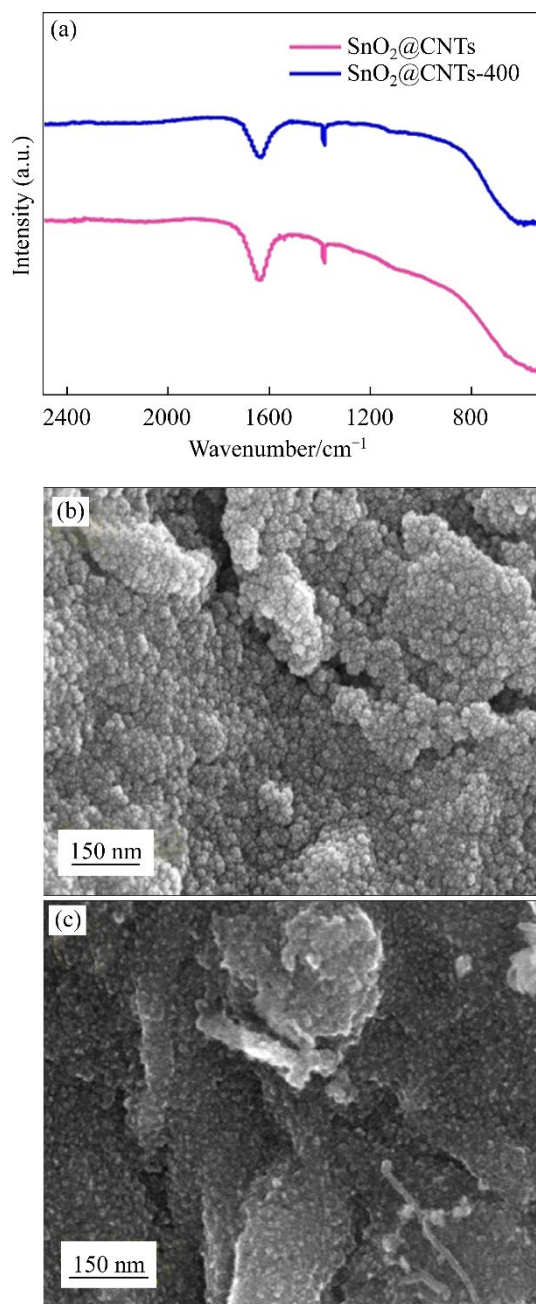


Figure S1 (a) The FT-IR spectroscopy of SnO₂@CNTs and SnO₂@CNTs-400; SEM images of (b) Sn/SnO₂ and (c) SnO₂@CNTs

2.2 XPS spectrum for SnO₂@CNTs

Figure S2(a) showed the chemical state and composition of SnO₂@CNTs, which is mainly composed of C, O, Sn elements. According to the high resolution of Sn 3d spectrum (Figure S2(b)), the binding energies of 487.7 eV and 496.1 eV corresponded to Sn 3d_{5/2} and Sn 3d_{3/2} of Sn⁴⁺, respectively [S2, S3]. The C 1s spectra at 285.14 eV and 289.3 eV were attributed to the C—O—C and O—C=O bonds [S4], which was consistent with the FT-IR spectroscopy (Figure S2(c)). For the spectrum of O 1s spectrum (Figure S3(d)), two peaks were observed at 531.4 eV and 532.8 eV, pointing to the Sn—O and Sn—O—C bonds, which confirmed the strong interfacial effect of the composite materials prepared by alternating current.

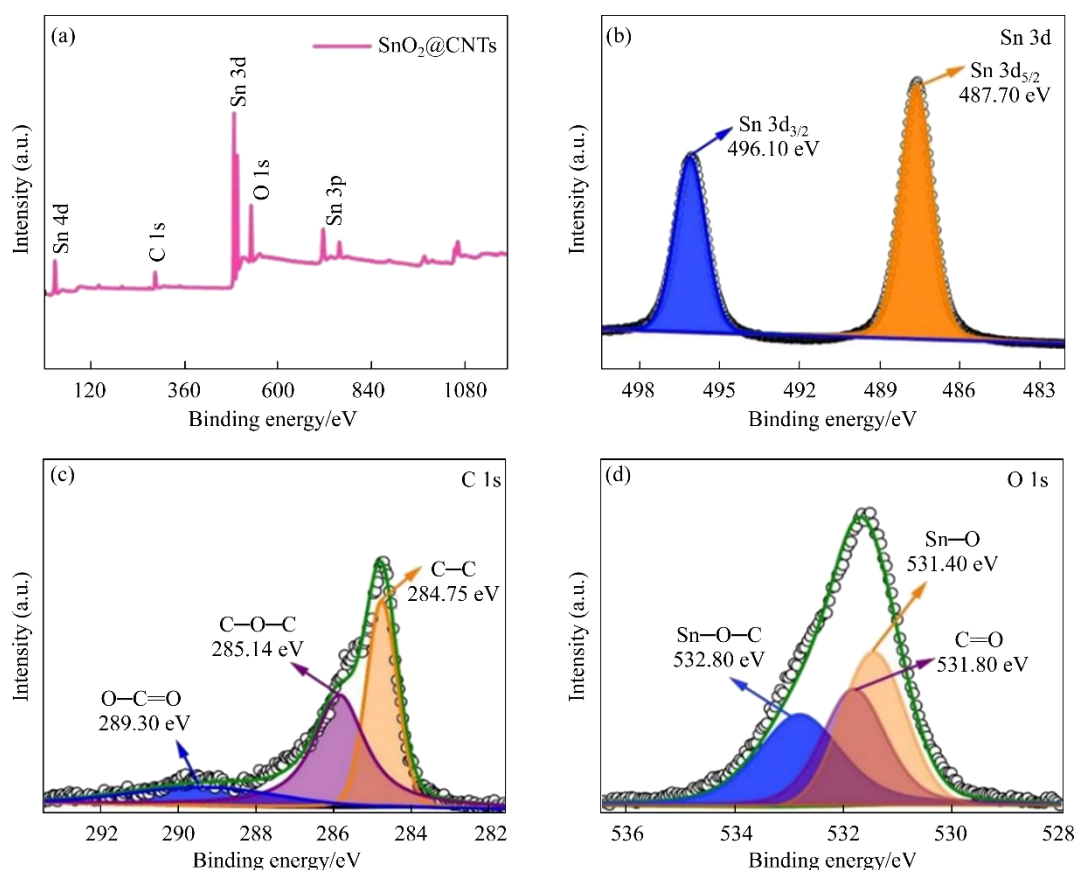


Figure S2 The XPS peaks exploration of SnO₂@CNTs: (a) Full spectrum; (b) Sn 3d spectrum; (c) C 1s spectrum; (d) O 1s spectrum

3 Electrochemical measurements

3.1 CV curves and GCD curves of SnO₂@CNTs

Obvious cathode and anode peaks appeared in CV curves, the cathode peak shifted from the second circle. The GCD curves had obvious charge and discharge platform, The capacity attenuation from the first circle to the second circle can be explained by the irreversibility of transformation reaction and the formation of the unstable SEI film [S5].

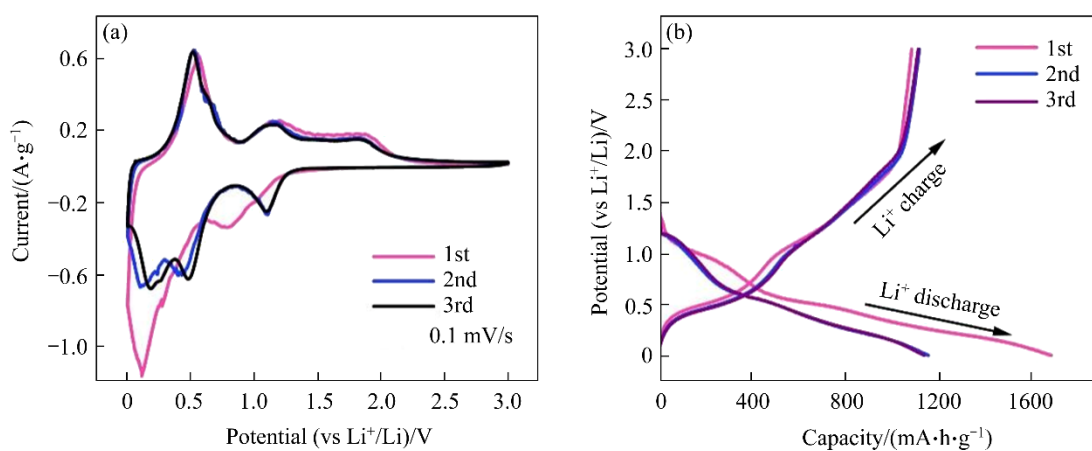


Figure S3 (a) CV curves at a scan rate of 0.1 mV/s of the SnO₂@CNTs; (b) First three cycles galvanostatic charge-discharge profiles at 0.1 A/g of the SnO₂@CNTs

3.2 GCD curves of SnO₂@CNTs at different current density

The magnification performance of SnO₂@CNTs was shown in Figure S4, with excellent reversible capacity of 1643.4 and 602.2 mA·h/g obtained at 0.1 and 3.2 A/g respectively.

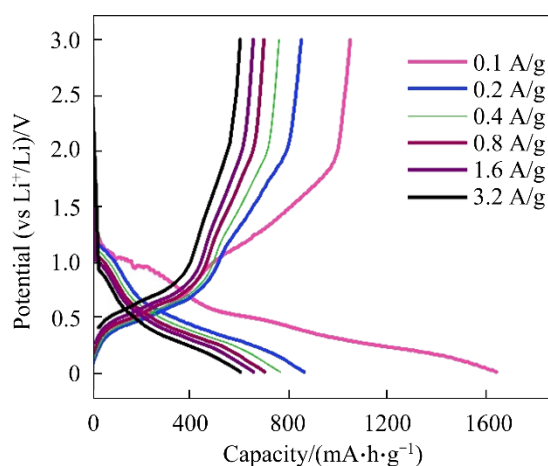


Figure S4 Galvanostatic charge-discharge profiles from rate performance of SnO₂@CNTs from 0.1 to 3.2 A/g

3.3 Cyclic curves of composite materials at 0.1 A/g

As shown in Figure S5, the specific capacities of the SnO₂@CNTs and SnO₂@CNTs-400 at the first discharge were 1682.4 and 1775.4 mA·h/g with the ICE of 63.1% and 64.5%, respectively. Both composite materials exhibited high specific capacity and cyclic stability. Due to the irreversible reduction of SnO₂ and formation of SEI film, the composite materials experience a significant capacity degradation from the first to the second cycle.

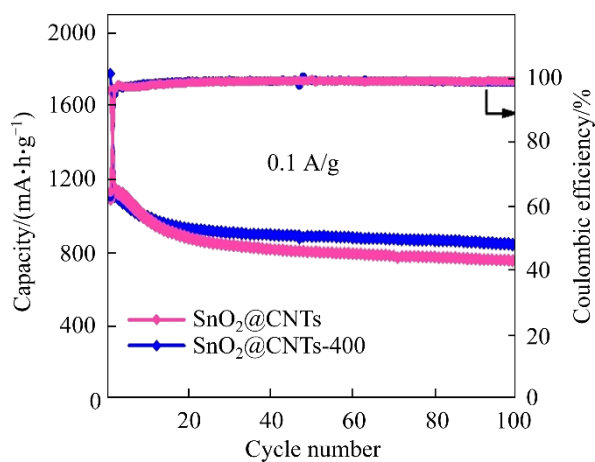


Figure S5 Cycling performance at a current rate of 0.1 A/g

3.4 CV curves at different scan rates and peak fitting slope

The four lines in Figure S6(b) were fitted by the redox peaks in Figure S6(a) respectively, and the *b* values of peak 1, peak 2, peak 3 and peak 4 were 1.24, 1.09, 1.03 and 0.87, respectively. The slope was close to 1, indicating the electrode capacity is mainly contributed by the surface capacitance [S6].

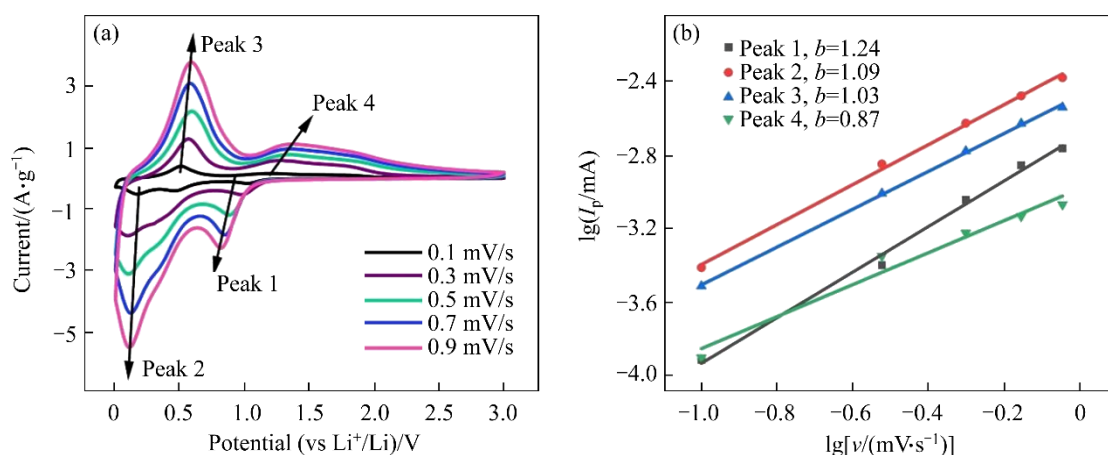


Figure S6 (a) CV curves at a series of scan rates of 0.1, 0.3, 0.5, 0.7 and 0.9 mV/s of the SnO₂@CNTs; (b) Slopes in the figure of the SnO₂@CNTs are fitted to the peak redox value in the CV curves

References

- [S1] BHATTACHARYA P, LEE J H, KAR K K, et al. Carambola-shaped SnO₂ wrapped in carbon nanotube network for high volumetric capacity and improved rate and cycle stability of lithium ion battery [J]. *Chemical Engineering Journal*, 2019, 369: 422–431. DOI: 10.1016/j.cej.2019.03.022.
- [S2] ZHANG Miao, SUN Zhen-he, ZHANG Teng-fei, et al. Excellent cycling stability with high SnO₂ loading on a three-dimensional graphene network for lithium ion batteries [J]. *Carbon*, 2016, 102: 32–38. DOI: 10.1016/j.carbon.2016.02.032.
- [S3] WANG Heng-guo, WU Qiong, WANG Ying-hui, et al. Molecular engineering of monodisperse SnO₂ nanocrystals anchored on doped graphene with high-performance lithium/sodium-storage properties in half/full cells [J]. *Advanced Energy Materials*, 2019, 9(3): 1802993. DOI: 10.1002/aenm.201802993.
- [S4] WANG Gui-zhi, FENG Jian-min, DONG Lei, et al. SnO₂ particles anchored on N-doped graphene surface as sodium-ion battery anode with enhanced electrochemical capability [J]. *Applied Surface Science*, 2017, 396: 269–277. DOI: 10.1016/j.apsusc.2016.10.109.
- [S5] ZHANG Wen, DU Rui, ZHOU Cheng-gang, et al. Ultrafine SnO₂ aggregates in interior of porous carbon nanotubes as high-performance anode materials of lithium-ion batteries [J]. *Materials Today Energy*, 2019, 12: 303–310. DOI: 10.1016/j.mtener.2019.02.003.
- [S6] WANG L P, LECONTE Y, FENG Zhen-xing, et al. Novel preparation of N-doped SnO₂ nanoparticles via laser-assisted pyrolysis: Demonstration of exceptional lithium storage properties [J]. *Advanced Materials*, 2017, 29(6): 1603286. DOI: 10.1002/adma.201603286.